Review article

Developments in the integration and application of terahertz spectroscopy with microfluidics

Salman Alfihed[a,b], Jonathan F. Holzman[a,*], Ian G. Foulds[a]

[a] *School of Engineering, University of British Columbia, Kelowna V1V1V7, Canada*
[b] *Materials Science Research Institute, King Abdulaziz City for Science and Technology, Riyadh 11442, Saudi Arabia*
[*] *Corresponding author. School of Engineering, University of British Columbia, Kelowna V1V1V7, Canada*
E-mail addresses: Jonathan.Holzman@ubc.ca

Abstract: This work presents an overview of terahertz (THz) spectroscopy with a focus on its implementation within microfluidic platforms. Such platforms are of great interest because they can enable label-free and reagent-free sensing. However, they must be implemented with thought towards the incorporated materials and structures as they can greatly impact the bandwidth, frequency resolution, signal-to-noise ratio, and dynamic range of the measurements. This review explores such relationships with insight given on the design and material considerations for the effective integration of THz spectroscopy in microfluidic platforms. The review also describes recent work on the application of THz spectroscopy to biomaterial analyses on increasing scales, targeting DNA, proteins, cells, and tissues.

Keywords: Terahertz time-domain spectroscopy; microfluidic platforms; biosensors.

1. Introduction

Terahertz (THz) technology has spurred numerous applications in medical (Philip et al., 2011) and biological sciences (Ajito et al., 2011). The applications come about from THz radiation's site in the electromagnetic spectrum between the domains of microwave and infrared radiation. Its wavelengths (100–1,000 μm) and frequencies (0.3–3.0 THz) cannot be generated by conventional electronic and optic technologies—and for this reason the generation and detection of THz radiation has been challenging in the past (Sirtori, 2002). In fact, its spectrum became known as the *THz gap*. This gap has since been filled by optoelectronic technologies (Defonzo and Lutz, 1987; Smith and Auston, 1988), which has led to numerous applications through the years (Exter et al., 1989; Exter and Grischkowsky, 1990; Hu and Nuss, 1995). The growth can be seen by the fact that the term *terahertz* has appeared within the title, abstract, or keywords of over 7000 research articles over 2016 to 2018.

During the growth in THz technology, there has been equally rapid growth in microfluidic technology (Whitesides, 2006). The developments started with the fabrication of the first microchip in the late 1970's (Goldstein et al., 1979) and have continued to this day in various forms

of microfluidic devices. Such devices can enable effective transport, mixing, separation, and detection of fluids with high selectivity and sensitivity (Whitesides, 2006).

Given the benefits of THz and microfluidic technologies, together, it is has become apparent that great benefits can be had by their integration. The benefits come about from the low photon energy of THz radiation, which yields resonant excitation with many biomolecular (vibrational and rotational) modes with negligible tissue damage (Dhillon et al., 2017), as well as the strong fluid-handling abilities of microfluidic devices. Ultimately, there is great potential to realize THz spectroscopy within microfluidic devices for highly effective biosensing (Yang et al., 2016b).

In this work, a review is given on the integration of THz spectroscopy and microfluidics towards the goal of realizing fully-integrated THz-biosensors. The foundational work of others, as well as our own work, is presented on the key design and material considerations—with attention given to their impact on the bandwidth, frequency resolution, signal-to-noise ratio (SNR), and dynamic range (DR). It is hoped that the presented work can lay the foundation for continuing advancements and future realizations of THz-biosensors.

2. Terahertz Spectroscopy

The foremost technique for realizing THz analyses is THz-time-domain spectroscopy (THz-TDS). The technique was introduced as a means to characterize the complex refractive index of materials as a function of frequency. It is accomplished by passing a broadband pulse of THz radiation through the material of interest and detecting the transmitted electric field. In this way, the material's characteristics for absorption and refraction are imparted onto the transmitted electric field's amplitude and phase, respectively (Ferguson and Zhang, 2002; Naftaly and Miles, 2005). The performance levels attained by THz-TDS in biomaterial characterizations are dictated by the effectiveness of generating and detecting THz radiation, as detailed in the appendix, and the effectiveness of the spectroscopic platform, as described in this section.

A representative THz-TDS system, with a microfluidic platform, is shown in Fig. 1. The system includes a photoconductive THz emitter and detector with the THz radiation (in yellow) focused through the microfluidic platform, shown expanded in the inset. The system has the incident pump beam (in red) generate the THz radiation. The generated THz radiation is collimated, focused, re-collimated, and focused via four parabolic mirrors. It is then sampled at the photoconductive THz detector by way of the coincident probe beam (in red). With such a system, the THz beam is focused through the microfluidic platform to maximize the material-induced refraction and absorption imparted onto the THz radiation. This is an important consideration for the characterization of materials with microscopic sizes, such as cells.

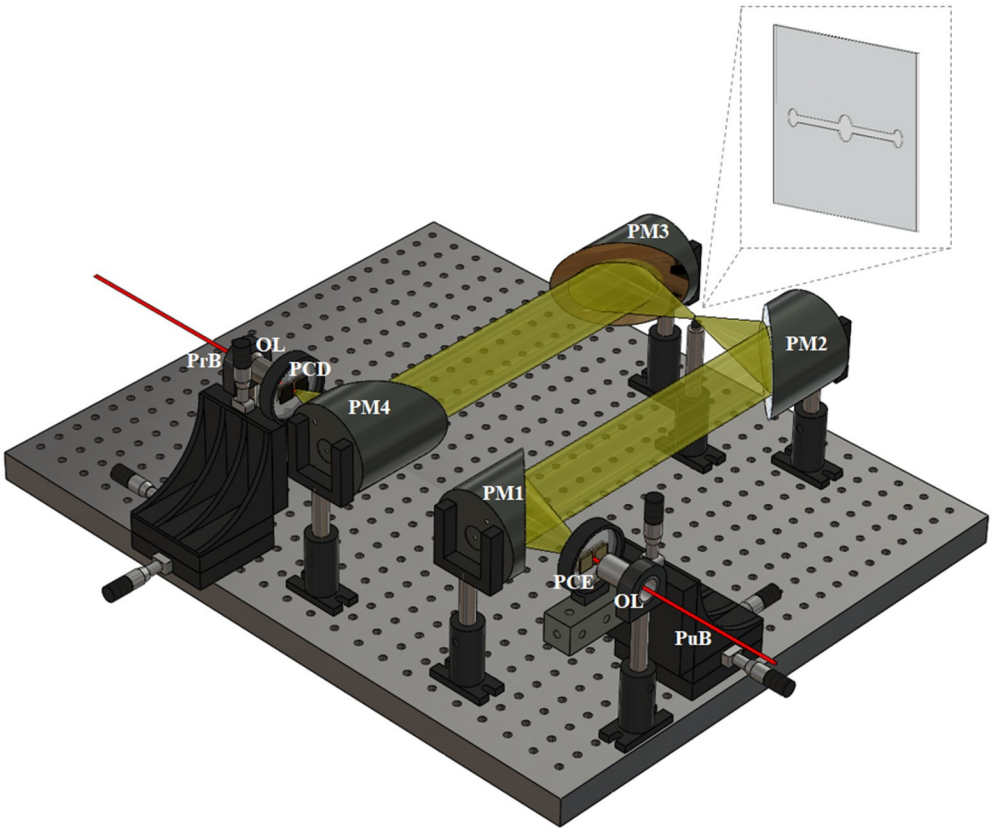

Fig. 1. A representative THz-TDS system with photoconductive THz generation and detection and a microfluidic platform. In the system, ultrashort laser pulses are delivered by the pump beam (PuB, in red) and probe beam (PrB, in red), which are each focused by an objective lens (OL) onto the photoconductive THz emitter (PCE) and photoconductive THz detector (PCD), respectively. The emitted THz radiation (in yellow) is collimated, focused, re-collimated, and focused by four parabolic mirrors (PM1-4) to allow the THz radiation to be focused through the microfluidic platform, shown expanded in the inset.

In a typical THz-TDS analysis with a microfluidic platform, the THz radiation passes through the microfluidic platform with and without the biomaterial of interest being present. The THz input waveform (entering the platform) then yields a THz sample waveform (exiting the platform with the biomaterial) and THz reference waveform (exiting the platform without the biomaterial). This lets the biomaterial-induced changes in amplitude and phase between the THz sample andreference waveforms be correlated to the biomaterial's absorption and refraction, respectively (Beard et al., 2002).

Terahertz radiation within the THz-TDS system is measured in the time domain as electric field waveforms. The waveforms are captured with the biomaterial present, yielding a THz sample waveform with an electric field of $E_s(t)$, and without the biomaterial present, yielding a THz reference waveform with an electric field of $E_r(t)$, versus time, t. The waveforms are Fourier transformed to define the complex-valued THz sample spectrum, $E_s(f)$, and THz reference

spectrum, $E_r(f)$, versus frequency, f. The transformation allows the frequency-dependent complex refractive index to be defined as $\tilde{n}(f) = n(f) - j\kappa(f)$, where $n(f)$ is the refractive index and $\kappa(f)$ is the extinction coefficient. The refractive index is defined by

$$n(f) = 1 + (c/2\pi f d)\,\mathrm{j}\arg\left(E_s(f)\right) - \arg\left(E_r(f)\right)\mathrm{j}, \quad (1)$$

where c is the free-space speed of light and d is the thickness of the biomaterial, corresponding to the microchannel depth when a microfluidic platform is used. The extinction coefficient is often redefined in terms of the (power) absorption coefficient as $\alpha(f) = 2k_0\kappa(f)$, where $k_0 = 2\pi f/c$ is the free-space wavenumber. Thus, the absorption coefficient of the biomaterial is

$$\alpha(f) = (2/d)\ln[(4n(f)/(n(f) + 1)^2)\mathrm{j}E_r(f)/E_s(f)\mathrm{j}]. \quad (2)$$

Note that the above two expressions neglect cascading internal reflections between the layers, although such reflections can be considered by following the approach of (Lesack et al., 2020). Ultimately, the accuracy of the extracted material parameters is dictated by the characteristics of the overall THz-TDS system, which can be defined by its bandwidth, frequency resolution, SNR, and DR (Withayachumnankul and Naftaly, 2014).

The typical bandwidth of a THz-TDS system spans 0.1 to 3.0 THz. However, many factors influence the bandwidth, including the laser pulse duration and physical form of the THz emitter and detector (Cunningham et al., 2011). While the laser pulse duration is often fixed for the laser system, the photoconductive material and electrodes can be adapted. Specifically, the material can be chosen to enable ultrafast photo-generation, transport, and recombination according to the details in (Burford and El-shenawee, 2017). The electrodes can be designed to maximize their bandwidth, as shown in (Cai et al., 1997), (Tani et al., 1997), and (Berry et al., 2013).

The frequency resolution is limited by two main parameters, the scanning delay time and noise level (Mickan et al., 2003; Withayachumnankul and Naftaly, 2014). The scanning delay time, as the maximum delay in time that the THz-TDS system imparts between the pump and probe pulses, corresponds to the duration of the time-resolved scan for the THz sample/reference waveform. The reciprocal of this scanning delay time sets the frequency resolution for the THz sample/reference spectra (Mickan et al., 2003). For example, a scanning delay time of 100 ps gives a frequency resolution of roughly 10 GHz. Longer scanning delay times can be used if finer frequency resolutions are desired, but the use of a laser pulse train within the THz-TDS system limits the frequency resolution to values above the pulsed laser's repetition rate. The noise level is an attribute of the THz-TDS system and its environment. When such noise is random, it becomes possible to implement averaging of the measurements to dampen this noise. In general, averaging can be implemented in the time or frequency domain—but the end results are not the same. It is found that noise is diminished to the greatest extent by carrying out the averaging in the time domain (Withayachumnankul and Naftaly, 2014). Such a trend can be seen in the results of Fig. 2. The

figure shows representative experimental results for the amplitude of THz sample/reference spectra as a function of frequency, *f*, with no averaging (dotted blue), averaging of 10 measurements within the frequency domain (solid orange), and averaging of 10 measurements within the time domain (solid yellow). It is apparent that the curves for no averaging and averaging in the frequency domain have similar noise floors, above roughly 2.0 THz, while the curve for averaging in the time domain has a reduced noise floor, being roughly three times lower than its counterparts. This shows the benefits of averaging the THz sample/reference waveforms prior to Fourier transforming into spectra.

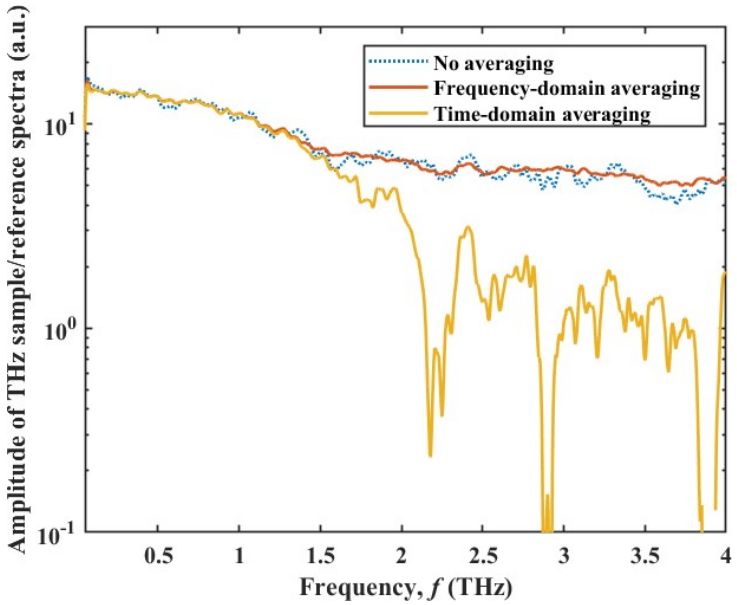

Fig. 2. Representative experimental results for the amplitude of a THz sample/reference spectrum as a function of frequency, *f*. The curves show results for no averaging (dotted blue), frequency-domain averaging (solid orange), and time-domain averaging (solid yellow).

The SNR is a characteristic that should be defined with caution. There is little agreement or standardization for it in the literature (Naftaly and Dudley, 2009). Nonetheless, the SNR can be rigorously defined by computing the Fourier transform of multiple THz sample/reference waveforms to produce a set of THz sample/reference spectra. The SNR is then the ratio of the mean signal amplitude (averaged across the frequency domain of all THz sample/reference spectra) to the standard deviation (computed across the frequency domains of all the THz sample/reference spectra) (Naftaly and Dudley, 2009). Note that the noise arising here manifests as random error and systematic error (Withayachumnankul et al., 2008b). Random error is seen as nondeterministic fluctuations in the THz sample/reference waveforms, and it leads to diminished precision. It is due to factors such as laser intensity fluctuation during the experiments and electronic noise. Systematic error is a result of experimental biases in the experimental system, and it leads to diminished accuracy. It is often due to imprecise experimental parameters, such as

error in the sample thickness, or nonideal experimental conditions, such as a misaligned sample orientation (Withayachumnankul et al., 2008b). In the first case, error in the sample thickness measurement leads to proportional systematic error in the extracted refractive index and extinction coefficient. In (Duvillaret et al., 1999), error in the sample thickness was characterized via standard divisions from 12 samples, and it was found to be the dominant contribution to systematic error in the extracted refractive index and extinction coefficient. The study used both thin and thick samples, and it was stated that the relative error of the thickness measurements should not exceed 1% to avoid large systematic errors in the extracted refractive index and extinction coefficient. In the second case, relating to misalignment in the sample orientation, the THz beam would propagate through the misaligned sample over an increased distance, being equal to the product of the true sample thickness, d, and the secant of the misalignment angle (Withayachumnankul et al., 2008b). Again, this error would lead to proportional systematic error in the extracted refractive index and extinction coefficient. Ultimately, the random and systematic errors together set an upper limit on the operational frequency, which occurs when the THz sample/reference spectra drop to the noise floor (Withayachumnankul et al., 2007). This limit leads to the definition of the dynamic range (DR).

The frequency-dependent DR, denoted in this work by DR(f), is a characteristic of the overall THz system and its noise. It is found by measuring the THz sample spectrum and normalizing the resulting curve by its noise floor (Jepsen and Fischer, 2005; Naftaly and Dudley, 2009). Such a definition makes it apparent that there is a maximum measurable absorption coefficient, $\alpha_{\max}(f)$, for each frequency that acts as an upper limit for the measured absorption coefficient, $\alpha(f)$, at that frequency (Jepsen and Fischer, 2005). With this in mind, the maximum measurable absorption, $\alpha_{\max}(f)$, and DR(f) can be related by

$$\alpha_{\max}(f) = (2/d)\ln[\mathrm{DR}(f)(4n(f)/(n(f)+1)^2)]. \quad (3)$$

Such an expression shows that materials will have optimal sample thicknesses for THz-TDS measurements. In (Withayachumnankul et al., 2008a) and (Duvillaret et al., 1999), the optimal sample thickness was proposed to be $2/\alpha(f)$, where $\alpha(f)$ is the absorption coefficient at the frequency, f, of foremost interest. For example, water has an absorption coefficient of approximately 200 cm^{-1} at 1.0 THz and so its optimal sample thickness is 100 μm. This interplay between the level of absorption and the sample thickness will play an important role in the upcoming analyses of microfluidic materials and platforms.

3. Material Considerations for Terahertz Spectroscopy via Microfluidic Platforms

The microfluidic platform, being the foundation for the applied microfluidic technology, enables the control of fluid transport, mixing, separation, and detection (Mark et al., 2010). This control is typically realized via microchannels in various materials. However, the type of material that is

used must be carefully considered in terms of transparency when it is applied to spectroscopy. The first generation of microchannels, having been fabricated out of silicon, yielded transparency only in the infrared spectrum. Later, microchannels were fabricated out of glass, enabling transparency across the visible spectrum and infrared spectrum, and for this reason glass remained as the foremost material for microchannels. Nonetheless, the amorphous morphology of glass leads to issues in precise etching of vertical sidewalls (Mcdonald et al., 2000), and high costs in some cases, and this has led to efforts to realize polymer-based microchannels. Polymers typically have low costs and if appropriately chosen can offer strong chemical stability (Tsao, 2016). However, the choice of polymers for THz spectroscopy must be made judiciously—with thought to absorption. The following subsections consider such absorption by characterizing and contrasting non-polymeric and polymeric materials.

3.1 Non-Polymeric Materials

Many non-polymeric materials, such as silicon and glasses, have been investigated via THz-TDS for frequencies ranging from 0.1 to 2.0 THz. High-resistivity silicon (HRSi) is particularly noteworthy because it shows far lower absorption than conventional silicon and many other materials. The absorption coefficients of HRSi are below 0.05 cm^{-1} between 0.1 to 2.0 THz (Dai et al., 2004). In contrast, quartz and silica exhibit absorption coefficients from 0.1 to 8 cm^{-1} at 2.0 THz, Pyrex exhibits absorption coefficients close to 30 cm^{-1} at 1.0 THz and 95 cm^{-1} at 2.0 THz, and BK7 glass exhibits absorption coefficients above 100 cm^{-1} at 1.0 THz (Naftaly and Miles, 2007a). The overall absorption characteristics as a function of frequency, f, can be seen in Fig. 3A for HRSi, quartz, silica, Pyrex, and BK7 in the range of 0.5 to 2.0 THz. Based on these results, and considerations of optical transparency, quartz and silica can be effective materials for integrating THz technology and microfluidics. Although, it should be noted that the network and structure of the silicate glasses can affect their absorption coefficients within the THz spectrum (Naftaly and Miles, 2007a, 2007b).

3.2 Polymeric Materials

Absorption coefficients of polymeric materials have also been investigated by THz-TDS. The polymers include polydimethylsiloxane (PDMS), polyimide, which may be referred to as Kapton, cyclic olefin polymer (COP) (or cyclic olefin copolymer (COC)), high-density polyethylene (HDPE), polystyrene (PS), polycarbonate (PC), and poly(methyl methacrylate) (PMMA), which may be referred to as Perspex.

Of the aforementioned polymers, PDMS is of particular interest due to its widespread use in microfluidics. However, characterizations of PDMS must be done with care given that the THz absorption characteristics can vary greatly with its preparation and curing conditions. The curing temperature, curing time, and cross-linker concentration, i.e., mass fraction, can all influence the mechanical properties (Johnston et al., 2014) and the absorption coefficient within the THz

spectrum (Alfihed et al., 2018b; Podzorov and Gallot, 2010). In particular, it has been found that an increasing cross-linker mass fraction in the PDMS mixture leads to a (slight) increase in the THz absorption coefficient. Podzorov and Gallot studied this for curing of PDMS with mass fractions of 3%, 5%, 10%, 15%, and 20% at 70°C for one hour. The absorption coefficient peaked at 1.3 THz for the mass fractions of 10%, 15%, and 20%, at roughly 11 cm^{-1}, but the absorption coefficient peaked at only 9 cm^{-1} for the mass fraction of 3% (Podzorov and Gallot, 2010). To understand the THz absorption of PDMS, the curing can be divided into two reactions. There is an initial reaction from which the two-vinyl end groups react with a multifunctional cross-linker, which results in a polymer network with a three-dimensional cross-linked structure. A post-curing reaction then follows. The post-curing reaction requires the presence of oxygen and its rate is dictated by the temperature. This reaction was studied deeply in (Quan, 1989), which showed that the cured polymer network does not follow the ideal polymer network when the curing process is carried out at elevated temperature. The resulting nonideality can affect both the mechanical and optical properties of the cured PDMS (Esteves et al., 2009). Our own studies on polymer cross-linking and THz absorption within PDMS have shown a correlation between the curing temperature and absorption coefficient—as well as a reduction in the post-curing reactions when the curing is carried out at reduced pressure (Alfihed et al., 2018b).

Absorption coefficients within the THz spectrum of the remaining polymers, including polyimide, COP (or COC), HDPE, PS, PC, and PMMA, have also been studied. Cunningham et al., examined the first three polymers, polyimide, COC, and HDPE for frequencies spanning 0.1 to 10 THz (Cunningham et al., 2011). The polyimide showed an absorption coefficient below 30 cm^{-1} in the range from 0.1 to 3.0 THz. A broad peak was observed in the range from 3.5 to 5.5 THz with an absorption coefficient that reached roughly 200 cm^{-1} at 5.0 THz. Another peak was observed near 7.9 THz with an absorption coefficient above 250 cm^{-1}. The COP showed a very low absorption coefficient, below 0.5 cm^{-1}, in the range from 0.1 to 1.0 THz. However, the absorption increased above this range and reached approximately 1.0 cm^{-1} at 3.0 THz. The HDPE showed a low absorption coefficient for THz frequencies, with absorption coefficients spanning 0.5 cm^{-1} to 30 cm^{-1} for frequencies in the range of 0.1 THz to 4.0 THz (Cunningham et al., 2011). Naftaly and Miles studied the absorption coefficient of the last three polymers, PS, PC, and PMMA, for frequencies spanning 0.1 to 2.5 THz (Naftaly and Miles, 2007a). The absorption coefficients for these polymers were approximately 3.1 cm^{-1} at 2.4 THz, 18 cm^{-1} at 1.5 THz, and 14 cm^{-1} at 1.0 THz for PS, PC, and PMMA, respectively. The full spectral results for the absorption coefficient of these materials are shown in Fig. 3A as a function of frequency, f, spanning 0.5 to 2.0 THz. The absorption coefficient for the four materials with the lowest losses, HRSi, COP, HDPE, and PS, are shown rescaled in Fig. 3B. It is important to note here that not all of these materials are transparent in the visible spectrum. Of the non-polymeric materials, HRSi is opaque, but silica, quartz, Pyrex, and BK7 are transparent. Of the polymeric materials, HDPE is opaque, while PDMS, polyimide, COP, PS, PC, and PMMA are transparent.

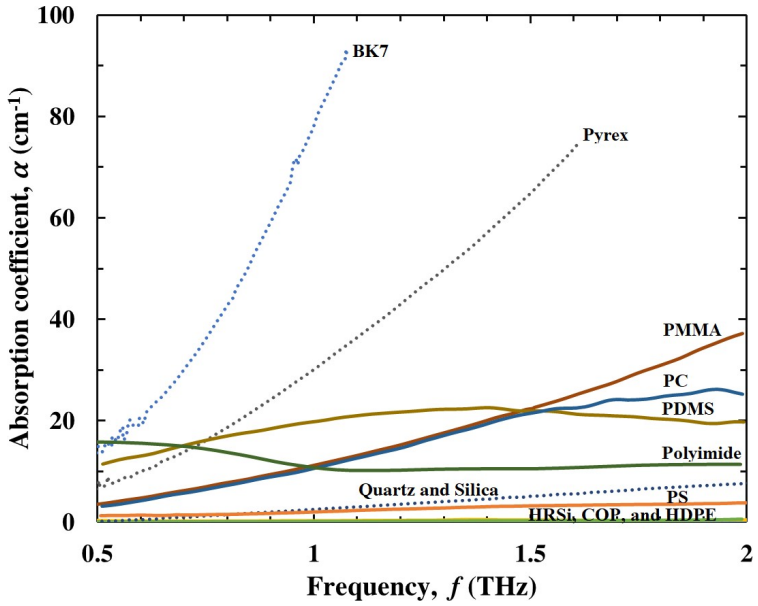

(A)

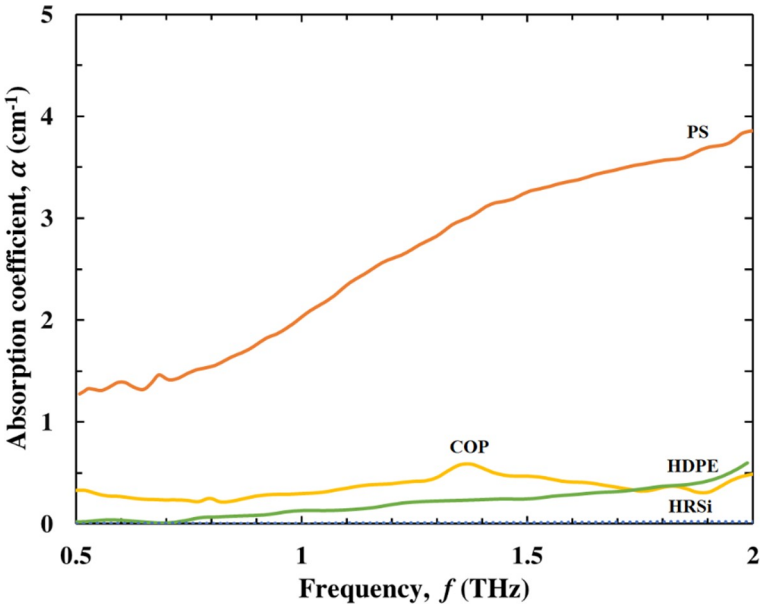

(B)

Fig. 3. Absorption coefficient as a function of frequency, *f*, between 0.5 to 2.0 THz for select non-polymeric and polymeric materials. In (A), the results are shown for select non-polymeric materials, HRSi (dotted blue), quartz and silica (dotted dark-blue), Pyrex (dotted grey), and BK7 (dotted light-blue), as well as select polymeric materials, PDMS (solid light-brown), polyimide (solid dark-green), COP (solid yellow), HDPE (solid green), PS (solid orange), PC (solid dark-blue), and PMMA (solid dark-brown). In (B), the results are shown for the lower-loss materials HRSi (dotted blue), COP (solid yellow), HDPE (solid green), and PS (solid orange). The presented data is from (Alfihed et al., 2018a; Dai et al., 2004; George et al., 2008; Naftaly and Miles, 2007a).

This visibility can be an important point when implementing the materials in a microfluidic platform. It is also important to note that the level of absorption in the polymers is a function of their chemical composition and crystallinity (Wietzke et al., 2011). Bershtein and Ryzhov considered various polymers morphologies by far-infrared spectroscopy and presented four types of macromolecular motion that influence the polymers' spectra (Bershtein and Ryzhov, 1994): skeletal vibrations, hydrogen bond oscillations, orientation polarization, and lattice modes.

Table 1 shows the THz absorption coefficient characteristics for all of the non-polymeric and polymeric materials along with the refractive indices of the materials. The refractive indices are included here because they can become a concern in microfluidic platforms if they lead to unacceptably high reflections. For example, HRSi shows low values for its absorption coefficient, but its refractive index is much higher than the other materials. This can lead to greater reflective losses from the platform as well as etalon artefacts, which appear as sinusoidal ringing within the measured THz spectra (Lesack et al., 2020).

Table 1

Select non-polymeric and polymeric materials' absorption coefficients at 0.5, 1.0, and 1.5 THz, listed from lowest to highest loss, and their refractive index averaged across 0.5 to 1.5 THz.

Material category	Material	THz absorption coefficient at 0.5 THz	THz absorption coefficient at 1.0 THz	THz absorption coefficient at 1.5 THz	Refractive index, 0.5 to 1.5 THz	Ref
Non-polymeric materials	HRSI	< 0.05 cm^{-1}	< 0.05 cm^{-1}	< 0.05 cm^{-1}	3.42	(Dai et al., 2004)
	Quartz	< 1 cm^{-1}	< 3 cm^{-1}	< 6 cm^{-1}	1.96	(Naftaly and Miles, 2007a, 2005)
	Silica	< 1 cm^{-1}	< 3 cm^{-1}	< 6 cm^{-1}	1.96	(Naftaly and Miles, 2007a, 2005)
	Pyrex	10 – 20 cm^{-1}	30 – 40 cm^{-1}	60 – 70 cm^{-1}	2.11	(Naftaly and Miles, 2007a)
	BK7	≈ 14 cm^{-1}	≈ 79 cm^{-1}	>100 cm^{-1}	2.50	(Naftaly and Miles, 2007a, 2005)
Polymeric materials	COP	< 0.4 cm^{-1}	< 0.4 cm^{-1}	< 1 cm^{-1}	1.52	(George et al., 2008)
	HDPE	< 0.5 cm^{-1}	< 1 cm^{-1}	< 1 cm^{-1}	1.54	(Cunningham et al., 2011; Naftaly and Miles, 2007a)
	PS	< 1 cm^{-1}	< 2 cm^{-1}	≈ 2 cm^{-1}	1.58	(Cunningham et al., 2011; Naftaly and Miles, 2007a)
	PDMS	≈ 4.5 cm^{-1}	≈ 9.2 cm^{-1}	≈ 10.5 cm^{-1}	1.59	(Alfihed et al., 2018b; Podzorov and Gallot, 2010)
	PC	≈ 3 cm^{-1}	≈ 10 cm^{-1}	≈ 18 cm^{-1}	1.63	(Naftaly and Miles, 2007a)
	PMMA	≈ 4 cm^{-1}	≈ 14 cm^{-1}	> 20 cm^{-1}	1.61	(Cunningham et al., 2011; Naftaly and Miles, 2007a)
	Polyimide	10 – 20 cm^{-1}	5 – 15 cm^{-1}	5 – 15 cm^{-1}	1.87	(Cunningham et al., 2011)

4. Design Considerations for Terahertz Spectroscopy via Microfluidic Platforms

The number of THz spectroscopic studies being carried out on biomaterials is growing. This is because the vibrational modes of many biomolecules, such as deoxyribonucleic acid (DNA) and proteins, have frequencies within the THz spectrum, and so THz spectroscopy can identify such biomolecules (Globus et al., 2006, 2003; Zhuang et al., 1990). Early studies of biomolecules at THz frequencies found that the high absorption of water over the THz spectrum restricted the analytical capabilities, and it became necessary to use dry samples (Nagel et al., 2002; Shumyatsky and Alfano, 2011). Later studies, using microfluidic platforms, showed that THz spectroscopy could be implemented in a highly effective manner through microchannels (Liu et al., 2013). The key benefits to the use of microfluidic systems over macroscale systems are an improved sensitivity, a broader spectrum, and a finer spatial resolution. The benefit of the improved sensitivity comes about from reduced water-induced absorption. This enables THz spectroscopy with less background absorption from the surrounding fluid and greater sensitivity to the targeted species (Tang et al., 2018; Yang et al., 2019). The benefit of a broader spectrum also comes about from reduced water-induced absorption, but its improvements are seen as an increased bandwidth. Here, the reduced absorption in a THz-microfluidic platform allows it to function up to higher frequencies simply because its noise floor is reached at a higher frequency (Baragwanath et al., 2010; Fan et al., 2016; Su et al., 2016). This gives an improved dynamic range and a broader spectrum. The benefit of a finer spatial resolution comes about because a THz-microfluidic platform can enable spectroscopy on a cellular level via near-field (subwavelength) functioning of its THz emitter and detector. The topic of spatial resolution is of growing interest in targeting single-cell analyses, and its details are shown elsewhere (Berrier et al., 2012; Reid et al., 2013; Tang et al., 2016; Yang et al., 2019).

Several pioneering studies on the combined use of THz radiation and microfluidic platforms have been carried out. The first study of THz imaging of the chemical concentration within fluid channels was demonstrated by (Kiwa et al., 2007), and the first studies of THz-microfluidic platforms were by (George et al., 2008) and (Baragwanath et al., 2010). These studies showed that THz-microfluidic platforms can be effective. However, the systems need to be carefully designed in terms of their structures, including the microchannel inlet/outlet, reaction/mixing chamber, and THz-TDS sampling site, and their (non-polymeric and polymeric) materials, as described in the following subsections. In general, these microfluidic devices can be realized as open or closed systems, but the choice of system should be made with consideration to their advantages and disadvantages. Open systems enable easy access and cleaning, but they can be sensitive to their environment or have varying thicknesses. This can make them subject to issues of repeatability. The issue of evaporation in open systems has been lessened by using humidified chambers or sacrificial water reservoirs (Barkal et al., 2016; Berthier et al., 2019, 2008). The issue of varying thicknesses has been be mitigated by using accurate theoretical models of the multilayered structures in sufficiently fast numerical routines, which process the theoretical and experimental

results to extract the refractive indices and extinction coefficients of all the layers. Our work has shown that THz transmission studies with these abilities can yield highly accurate characteristics of samples with time-varying thicknesses (Lesack et al., 2020). Closed systems are less sensitive to their environment and have relatively static thicknesses, but their performance can degrade without effective cleaning. Such cleaning can be realized by solvent injection or disassembly. To implement solvent injection, ethanol, deionized water, phosphate buffers, and/or air have been driven through microfluidic devices to enable multicycle (and even programmable) cleaning (Lorenzo Amato et al., 2012; Wang et al., 2020; Yu et al., 2015). To allow for device disassembly, various microfluidic devices have been developed with removable layers that can be detached for access and cleaning (Dalton and Kaler, 2007; Lin et al., 2013).

4.1 Non-Polymeric Terahertz-Microfluidic Platforms

Terahertz-microfluidic platforms have been fabricated and tested using non-polymeric materials, with a focus on silicon and quartz.

A silicon-based THz-microfluidic platform was used to detect the time-varying refractive index of various isopropanol/water mixtures for spectra spanning 0.5 to 3.0 THz (Baragwanath et al., 2010). This platform is shown in Fig. 4A as an exploded view. It is comprised of two metal plates that are used to clamp the PDMS gaskets onto the silicon-based microfluidic platform, while aligned to an inlet and outlet. The two metal plates have windows to allow the THz radiation to pass through the THz-microfluidic platform. Such a platform benefits from the precision with which microchannels can be etched in the silicon. As an example of this concept, a silicon photonic crystal array was used to characterize THz transmission spectra of ethanol, acetone, and petroleum ether spanning 0.3 to 1.9 THz (Fan et al., 2013). The array was fabricated by dry etching a 400-μm thick silicon wafer to form two distinct silicon-based THz-microfluidic platforms. Such platforms are promising for real-time quantitative sensing of biomaterials. However, silicon is opaque for the visible spectrum, and so it becomes challenging to monitor the flow of fluids. With such visibility in mind, alternative materials such as quartz have been considered for microfluidic platforms.

A quartz-based THz-microfluidic platform was used for chemical sensing over 0.57 to 0.63 THz (Liu et al., 2016). The fabricated platform, shown in Fig. 4B, consisted of four microchannels with a 50-μm depth, two quartz slides with a 1-mm thickness, and two PDMS slabs bonded onto the quartz, which had inlets and outlets for the microchannels. A variety of isopropanol/water and acetonitrile/water mixtures were tested in this platform. It was found that the quartz slides had minimal influence on the sensing capabilities of the platform (Liu et al., 2013). At the same time, the quartz was transparent in the visible spectrum, which allowed for monitoring of the fluids.

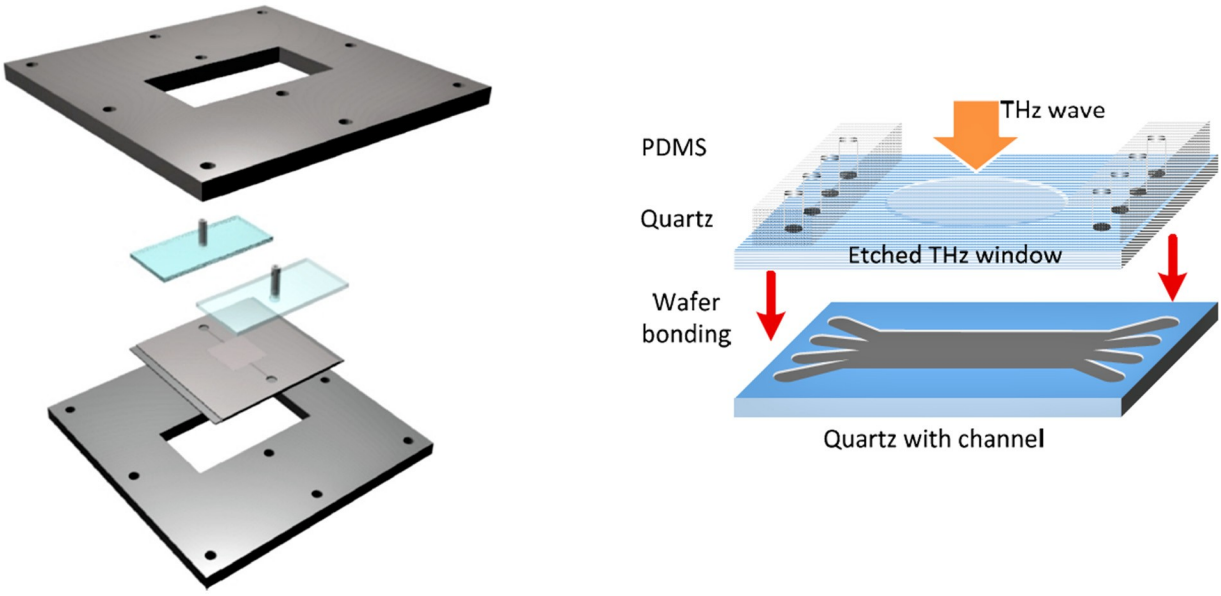

(A) (B)

Fig. 4. Examples of THz-microfluidic platforms based upon non-polymeric materials. In (A), a silicon-based THz-microfluidic platform is shown. It consists of two metal plates that are used to clamp the PDMS, while aligned to an inlet and outlet, into the silicon-based microfluidic platform. The windows within the metal plates allow the THz radiation to pass through the THz-microfluidic platform. This figure is reprinted from (Baragwanath et al., 2010) with the permission of AIP Publishing. In (B), a quartz-based THz-microfluidic platform is shown. It consists of four microchannels, two quartz slides, and two PDMS slabs bonded onto the quartz, with inlets and outlets for the microchannels. This figure is reprinted from (Liu et al., 2016).

4.2 Polymeric Terahertz-Microfluidic Platforms

Polymers can be advantageous for the implementation of THz-microfluidic platforms, and the use of such materials is considered in this section.

A common polymer for microfluidic applications is PDMS. It is permeable to gases, which enables the supply of oxygen and buffering to cells (Halldorsson et al., 2015), and thus enables the manipulation of live cells. An early prototype of a PDMS-based THz-microfluidic platform was studied by Tang et al., for the realization of cell trapping (Tang et al., 2016, 2013). The researchers used the THz-microfluidic platform shown in Fig. 5A. The platform was fabricated based on a 1.44-mm-thick PDMS layer. The PDMS layer contained a 300-µm-thick channel having two electrodes that were deposited on a glass substrate. The two electrodes were used to trap a given cell by way of their non-uniform electric field and dielectrophoretic force. Such a force transports the targeted cell to the high electric field region if it has a higher polarizability than its surroundings and to the low electric field region if it has a lower polarizability than its surroundings. The experiment made use of several steps: scanning of the metal aperture as a reference, scanning of the empty channel, scanning of the channel with a cell, and scanning of a trapped cell (with the applied electric field). The work showed the proof-of-concept realization of cell-trapping and THz

spectroscopy (Tang et al., 2016). Nonetheless, future implementations of such studies must consider the relatively high absorption of PDMS within the THz spectrum. As such, COP has been considered as a low-loss polymer in lieu of PDMS for THz-microfluidic platforms (George et al., 2008).

A variety of COP-based THz-microfluidic platforms have been fabricated for biomolecular detection via THz spectroscopy. As an early prototype, a COP-based platform was designed to detect changes in concentration of the protein bovine serum albumin (BSA) within a phosphate buffer (George et al., 2008). Its fabrication was based on hot-embossing of the polymer with a silicon template. A 95-µm-deep channel was fabricated in a COP layer and then capped with a second COP layer. Thermal annealing was then used to bond the layers and form the channel. The complete platform is showed in Fig. 5B. It consists of a sample input, reagent inputs, a reaction chamber to react the sample with the reagents, a detection chamber (THz-TDS sampling site) in which the THz radiation is passed through, and the output. A COP-based platform was later developed by Su et al., for the study of amino acids in aqueous solutions via THz-TDS (Su et al., 2016). It was implemented in a similar manner to that described above, albeit with a slightly modified platform. Their THz-microfluidic platform had two 2-mm-thick COP layers and a 10-µm-thick positive photoresist (PR1-4000A) layer. The platform consisted of an inlet, an outlet, and a THz-TDS sampling site. The fabricated platform was used to detect the amino acids L-threonine and L-arginine in the spectrum spanning 0.2 to 2.8 THz. More recently, a THz-microfluidic platform was fabricated with COP and used to detect glycerol (Bo et al., 2018). The platform had a microchannel formed from PDMS capped by two COP layers, which were used as low-loss THz windows over a detection area with a 3.5-mm diameter.

The influence of material absorption in THz-microfluidic platforms is a key point and is worthy of study. In our work, we fabricated THz-microfluidic platforms based on polyethylene terephthalate (PET), as a polar polymer with relatively high absorption, and ultra-high-molecular-weight polyethylene (UHMWPE), as a nonpolar polymer with relatively low absorption (Alfihed et al., 2018a). We found that the THz-microfluidic platform based upon the high-absorption PET polymer could yield a bandwidth of only 1.38 THz, while the THz-microfluidic platform based upon the low-absorption UHMWPE could yield a bandwidth of 1.75 THz. The bandwidth improvement seen here for the UHMWPE platform was attributed to its lower absorption, which gave higher signal levels and greater DR values in comparison to those of the PET platform. The influence of material absorption in THz-microfluidic platforms was also characterized in (Al-hujazy and Collier, 2018). This study showed the relationship between the thickness of a THz-microfluidic platform and its resulting DR. In general, the maximum measurable frequency increases as the platform's thickness decreases. This is due to the decreased absorption, increased signal levels, and thus increased DR values, as described earlier. This is an important issue when targeting biomolecular absorption peaks at higher frequencies, such as the L-glucose peak at 2.12

THz and the D-glucose at 2.1 THz (Upadhya et al., 2003). In such cases, it can become necessary to use very thin materials in the THz-microfluidic platform.

The results from studies with THz-microfluidic platforms over the past decade are shown Table 2. The table shows the measurement bandwidths of the THz-microfluidic platforms in carrying out spectroscopic measurements for differing platform materials and fabrication processes. Note that quartz, PDMS, and COP are the most commonly used materials for the integration of THz spectroscopy within microfluidic platforms.

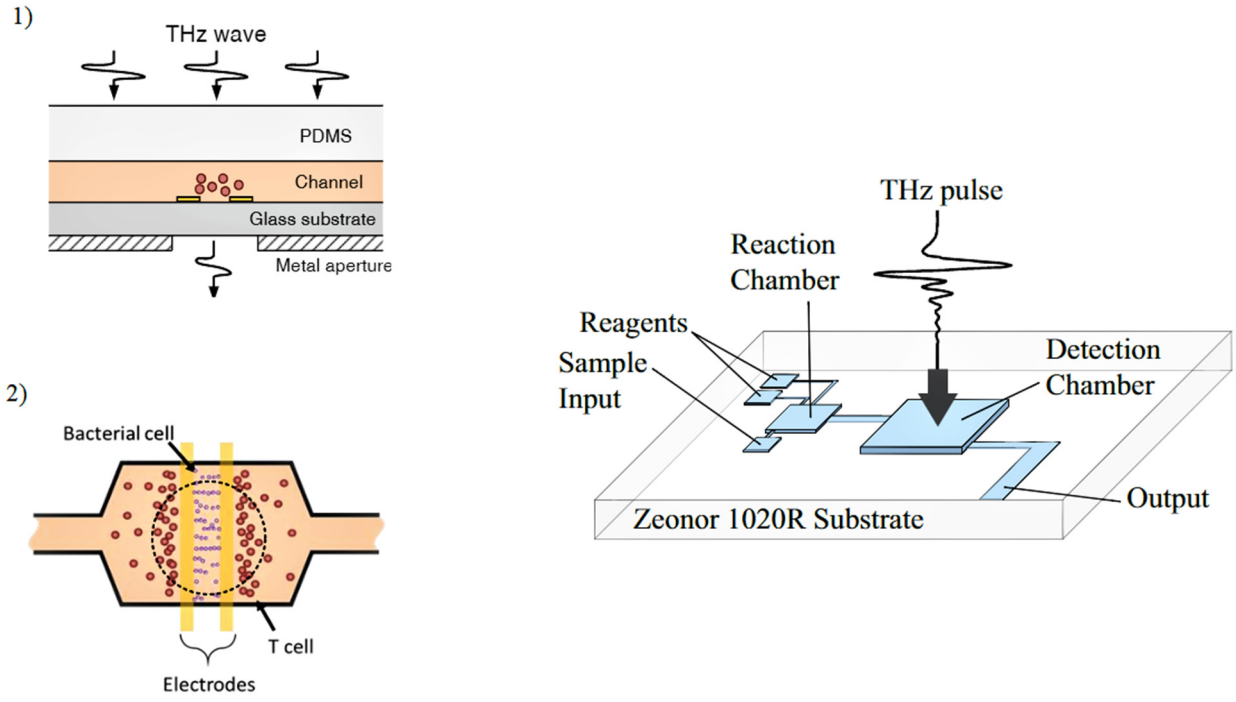

(A) (B)

Fig. 5. Examples of THz-microfluidic platforms based upon polymeric materials. In (A), a PDMS-based THz-microfluidic platform is shown. Diagram 1) shows its glass substrate, PDMS layer with a 300-µm-thick channel, and two gold electrodes, between which cells are trapped. Diagram 2) shows a top view of the microfluidic platform after applying voltage to the electrodes. This figure is reprinted (with a slight modification) from (Tang et al., 2016). In (B), a COP-based THz-microfluidic platform is shown. It consists of a sample input, reagents, a reaction chamber to react the sample with the reagents, a detection chamber in which THz radiation is passed through, and the output. This figure is reprinted with permission from (George et al., 2008) © The Optical Society.

Table 2

Published work on the integration of THz spectroscopy and microfluidic platforms, in terms of the platform material, fabrication process, spectroscopic measurement, and measurement bandwidth.

Platform material	Fabrication process	Spectroscopic measurement	Measurement bandwidth (THz)	Ref
Silicon	Etching	Isopropanol/water	0.5 – 3.0	(Baragwanath et al., 2010)
Silicon	Etching	Ethanol, acetone, and petroleum ether	0.3 – 1.9	(Fan et al., 2013)
Quartz	Etching	Isopropanol/water and acetonitrile/water	0.57 – 0.63	(Liu et al., 2016)
Quartz	Etching	Isopropanol/water	0.57 – 0.63	(Liu et al., 2013)
Quartz and photoresist	Photolithography and laser drilling	DNA oligonucleotides	0.6 – 1.4	(Tang et al., 2018)
Quartz and cured SU-8	Soft lithography	Deionized water	0.1 – 1.5	(M. Liu et al., 2016)
PDMS on a glass substrate	Soft lithography	Cell concentration	0.1 – 0.5	(Tang et al., 2016, 2013)
PDMS	Soft lithography	Detection of water flow	0.25 – 0.75	(Song et al., 2017)
PDMS and COP	Soft lithography	Glycerol	0.2 – 1.4	(Bo et al., 2018)
PDMS and COP	Soft lithography	Isopropanol/water	0.2 – 2.6	(Fan et al., 2016)
PET and COP	Milling cutter	Living cells measurements	0.3 – 2.0	(Yang et al., 2019)
PET and COP	Milling cutter	Bacterial DNA detection	0.3 – 2.0	(Yang et al., 2017)
COP	Hot-embossing	Bovine serum albumin in a phosphate buffer	0.5 – 2.5	(George et al., 2008)
COP and photoresist (PR1-4000A)	Photolithography	L-threonine and L-arginine	0.2 – 2.8	(Su et al., 2016)
UHMWPE/PET and PMMA	Laser cutter	PDMS curing-agent	0.5 – 2.0	(Alfihed et al., 2018a)

5. Bio-applications of Terahertz Spectroscopy

Terahertz spectroscopy is a multidisciplinary research field with growing attention. Based upon the Web-of-Science database over the past 10 years, the number of citations per year of the terms "terahertz" and "bio" has increased six-fold, from 150 citations in 2008 to 930 citations in 2018, while the number of citations per year of "terahertz" and "microfluidic" has increased 20-fold, from only 10 citations in 2008 to 201 citations in 2018. The growth can be seen in Figs. 6A and B, which show the numbers of the citations per year for the above-stated pairs of terms. In light ofthis growth, the following subsections show the trend towards integration of THz and microfluidic technologies in spectroscopic characterizations of DNA, proteins, cells, and tissues.

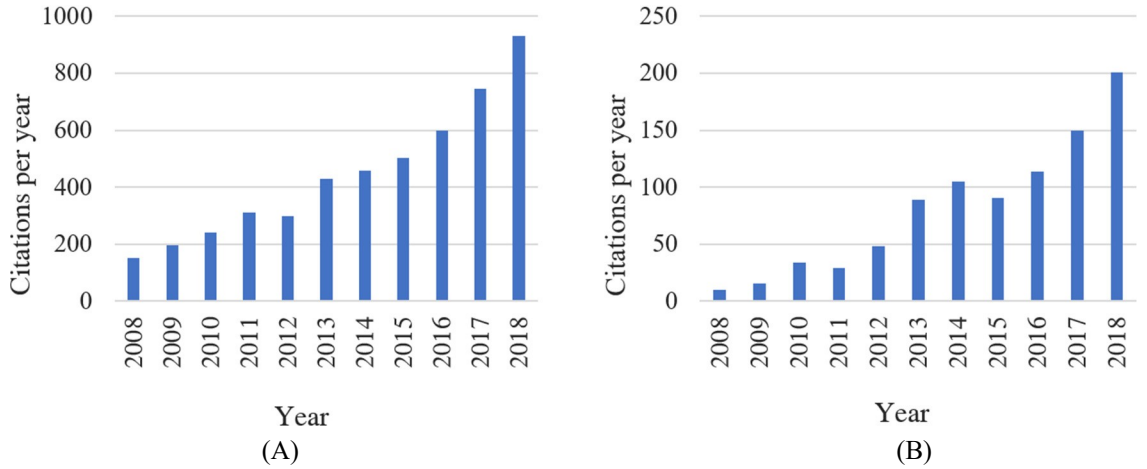

Fig. 6. Citations per year over 2008 to 2018 with the terms (A) "terahertz" together with "bio" and (B) "terahertz" together with "microfluidic". The presented data is from the Web-of-Science database.

5.1 Terahertz Spectroscopy on DNA

The vibrational modes of DNA can be seen in the THz spectrum, which has led to a great deal of interest from the applied THz research community. Early research on this topic made use of pressed pellets as samples. Markelz et al. presented characterizations of lyophilized powder samples of calf thymus DNA from 0.06 to 2.0 THz (Markelz et al., 2000), while Fischer et al., studied the building blocks of DNA by way of THz spectroscopy over 0.5 to 4.0 THz (Fischer et al., 2002). The results showed that the spectral absorption features of the DNA are related largely to hydrogen bonds between molecules. The work of (Cheon et al., 2016) showed molecular resonance in DNA from cancer cell lines. The liquid samples were frozen and then placed in a mount with quartz window, while held at a temperature of 253 K during the characterizations. The samples' THz absorption spectra were then collected over 0.4 to 2.5 THz. More recently, the implementations moved towards microfluidic platforms. For example, Tang et al., developed a quartz-based THz-microfluidic platform to study short DNA chains, i.e., oligonucleotides, over 0.6 to 1.4 THz (Tang et al., 2018). The researchers used a microfluidic platform with 50-µm-thick channels and liquid samples of DNA oligonucleotides with low water content. They studied four

different DNA oligonucleotides and showed that the oligonucleotides give distinct absorption spectra due to their differing numbers of hydrogen bonds.

5.2 Terahertz Spectroscopy on Proteins

Several THz spectroscopic characterizations have been carried out on proteins in the form of solid samples or aqueous solutions (in THz-microfluidic platforms). For example, (Chen et al., 2005) prepared 45-μm-thick films between two quartz layers and studied the oxidation state of the cytochrome c protein in absorption spectra up to 2.4 THz. The results showed correlation between the oxidation state and THz absorption coefficient. Later, (Zhang and Durbin, 2006) studied the influence of water content in the myoglobin protein over 0.1 to 1.2 THz. They used samples of myoglobin powder with differing water content, sandwiched between HDPE layers, and found that samples with higher water content had far higher THz absorption coefficients. Subsequently, protein characterizations were carried out by (George et al., 2008) in a THz-microfluidic platform with a 95-μm-thick channel containing BSA between two COP layers. The study had varying concentrations of BSA in a phosphate buffer with spectra spanning 0.5 to 2.5 THz. Ultimately, it was found that THz absorption increases as the BSA concentration decreases.

5.3 Terahertz Spectroscopy on Cells

Microscopic bacteria and cellular investigations have also been carried out by way of THz spectroscopy—and with great success. For example, five bacterial species were studied on quartz substrates with the sensitivity improved by way of plasmonic antennas (Berrier et al., 2012). The sensitivity and thus the limit of detection was enhanced by the antennas, which greatly aided identification of the differing bacterial species. Subsequently, (Yang et al., 2016a) analysed the bacteria *A. baumannii*, *P. aeruginosa*, *E. coli*, and *S. aureus* in spectra spanning 0.2 to 2 THz. It was found that the absorption coefficient at 2 THz varied from approximately 900 cm^{-1} for *A. baumannii* to below 500 cm^{-1} for *S. aureus* bacteria. Such variation showed the effectiveness of bacteria identification—with prospects for the control of infectious diseases because the analyses are rapid and label-free. More recently, the dielectric constant of *E. coli* bacteria was studied over 0.5 to 2.5 THz by (Yoon et al., 2020). The samples were prepared as stacks of microbial films with overall thicknesses of 200 to 600 μm. It was found that the microorganisms' differing cellular structures gave distinct dielectric properties that can be used for identification.

Terahertz spectroscopic studies have also been used to characterize cellular growth and properties. For example, it has been shown that there is correlation between vascular endothelial growth factor and the THz absorption coefficient, which can be characterized and used to identify minute changes in cell monolayers (Liu et al., 2007). To this end, Shiraga et al. studied the complex dielectric constants of three cancer cell lines via THz spectroscopy. The cells were characterized via spectroscopy over 0.2 to 4.0 THz. The results showed minor variations in dielectric constant between the three cancer cells (Shiraga et al., 2014). Much work has also been done on the study

of human blood cells via THz spectroscopy. For example, (Reid et al., 2013) studied the absorption spectrum of the blood cells and compared it to spectra of water and hemoglobin molecules over 0.25 to 2.0 THz. The measurements were carried out on three liquid samples with a microfluidic platform having two quartz windows. The thickness of the platform was varied between 100 and 1,000 µm by way of a Teflon spacer. It was shown that the absorption spectrum of the blood cells spanned the range between the spectra of the water and hemoglobin molecules. More recently, living cells were characterized via THz spectroscopy within a microfluidic platform (Yang et al., 2019). The employed THz-microfluidic platform is shown in Fig. 7A. It made use of PET and COP within a structure having two 1,000-µm-thick COP layers as windows bonded to a 100-µm-thick PET layer. The PET layer included a 200-µm-wide microchannel. The cells were injected through the microchannel into a hexagonal detection area and cultured for 12 hours. Low-viscosity oils were then injected as optical clearing agents. (Oils were used here in lieu of water to give low background levels of THz absorption.) The study characterized human breast cancer cells with silicon oil, fluorinated oil, and mineral oil. The results are shown in Fig. 7B as the absorption coefficient versus frequency. The results show that mineral oil yields the lowest absorption coefficients, and thus the best results. Ultimately, it can be concluded from such results that THz spectroscopy can be carried out on cells within microfluidic platforms while realizing sensitive measurements. Such functionality avoids the need for (and the unwanted effects of) dehydrating samples, which must often be done in working with macroscopic tissues.

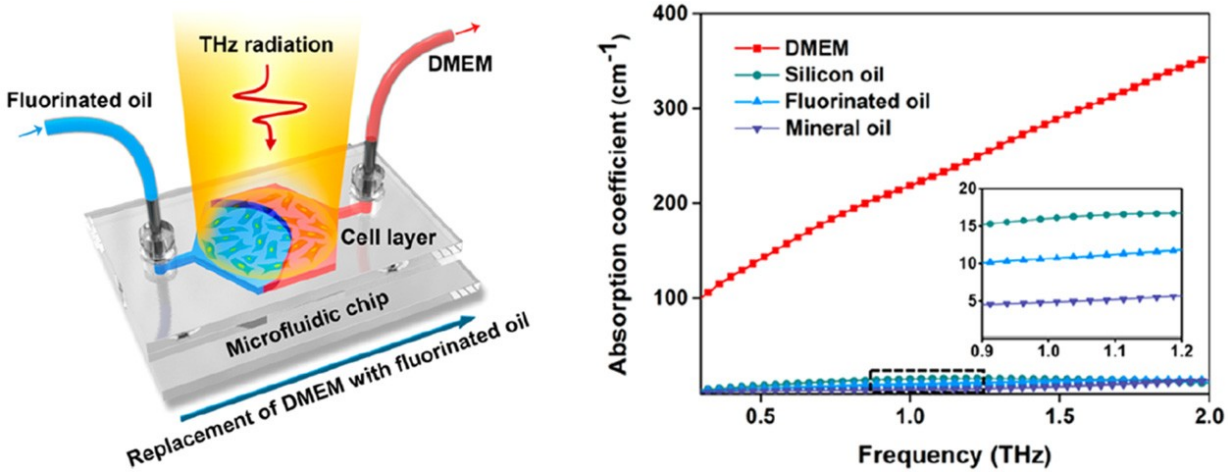

(A) (B)

Fig. 7. Implementation of THz spectroscopy on living cells with a microfluidic platform (Yang et al., 2019). In (A), the platform is shown with two COP layers as THz windows bonded to a 100-µm-thick PET layer with 200-µm-wide microchannels. It is shown with fluorinated oil in its inlet, a hexagonal detection area, and an outlet for the Dulbecco's modified Eagle's medium (DMEM). In (B), results for the absorption coefficient versus frequency are shown for the DMEM, silicon oil, fluorinated oil, and mineral oil. The figure is reprinted (slightly modified) with permission from (Yang et al., 2019). Copyright (2019) American Chemical Society.

5.4 Terahertz Spectroscopy on Tissues

Macroscopic tissue characterizations have also been carried out by THz spectroscopy—while often targeting label- and reagent-free detection for early diagnoses (Yu et al., 2019). For example, human tooth tissues were characterized while targeting distinct sites, including dentine and enamel (Nazarov et al., 2008). The THz absorption coefficients recorded for such sites over 0.3 to 2.5 THz showed the ability to distinguish the differing tissues. Furthermore, (Ashworth et al., 2009) characterized the refractive and absorptive characteristics of human breast cancer tissues for 20 patients in the range 0.15 to 2.0 THz. The samples were refrigerated to fix the moisture content and were sliced to give a fixed thickness. The results showed that healthy tissues have lower refractive indices and absorption coefficients on average, as a proof-of-concept in distinguishing healthy and cancerous tissues via THz spectroscopy. Frozen human brain tissues have also been studied in the THz spectrum to distinguish between healthy tissues and those subject to Alzheimer's disease. It was shown in (Png et al., 2009), for example, that the differing protein structures of healthy and diseased tissues are linked to differing vibrational modes, which can be seen as distinct signatures in the refractive index and absorption coefficient within the THz spectrum. Human skin tissues have also been studied by a somewhat portable THz spectroscopy system operating over 0.1 to 2.0 THz (Grundt et al., 2013). The system measured the hydration level of skin tissues, and it was found to benefit from the low scattered loss associated with the relatively long wavelengths of THz radiation. Nonetheless, all of the above tissue characterizations were implemented on macroscopic tissue samples, without disaggregation, and so their realizations via microfluidic platforms are largely unrealized. This point was made Yang et al., in *Trends in Biotechnology*, within which the authors give a call-to-action for further developments on the integration of THz spectroscopy and microfluidic platforms (Yang et al., 2016b).

6. Conclusions

This work presented a review of research towards the integration of THz spectroscopy within microfluidic platforms. Such work is of growing interest given the potential of THz spectroscopy for label-free and reagent-free sensing and the capabilities of microfluidic technology for high-sensitivity and high-selectivity measurements. Nonetheless, the materials and structures for such platforms must be chosen judiciously to meet the unique demands of the THz spectrum. The structures and materials together dictate the level of THz absorption within the platform, which sets the bandwidth, frequency resolution, SNR, and DR. Structures based upon non-polymeric materials such as HRSi and quartz were shown to bring about effective performance, in terms of these metrics, although structures based upon polymeric materials are becoming strong competitors. This is because polymers such as COP and HDPE yield low THz absorption, for strong performance, along with practical benefits such as low costs. The results from pioneering biological studies with THz-microfluidic platforms were also summarized in this work. The studies showed that the integrated nature of such platforms can bring about lower levels of water

absorption in the THz spectrum and improved spectroscopic performance. This could be seen in recent THz spectroscopic characterizations on increasing scales, targeting DNA, proteins, cells, and tissues. Overall, it can be concluded that there is growing interest and even greater potential for the integration of THz spectroscopy within microfluidic platforms.

Acknowledgements

This work was supported by the Natural Sciences and Engineering Research Council of Canada (RGPIN-2015-06711 and RGPIN-2017-04073), Canadian Foundation for Innovation (16659 and 34105), and Western Economic Diversification.

Appendix. Generation and Detection of Terahertz Radiation

Terahertz radiation can be generated by two main approaches, photoconductive generation and optical rectification. For photoconductive generation, THz radiation is generated when ultrashort laser pulses with above-bandgap photon energies are incident onto a biased photoconductive antenna. The photo-generated electron-hole pairs accelerate in the bias field, and this radiates electromagnetic waves with frequencies spanning the THz spectrum. The effectiveness of this radiative process can be improved by matching the photoconductor to free-space with a photoconductive antenna. The photoconductive antenna is typically formed on a semi-insulating semiconductor substrate with two metal electrodes separated by a photoconductive gap. The geometry of the electrodes and photoconductive antenna as a whole plays an important role in the performance of the photoconductive generation process (Tani et al., 2012). For optical rectification, ultrashort laser pulses are also used, but in this case they are made to propagate through a nonlinear electro-optic crystal. This brings about a second-order (Pockels) nonlinearity with a nonlinear polarization having a quasi-static component. The quasi-static component follows the ultrashort laser pulse's envelope, which forms a subpicosecond electromagnetic pulse with a broadband (THz) spectrum (Jin et al., 1994).

Terahertz radiation can be detected by two approaches, photoconductive detection and electro-optic detection, which parallel the approaches for generation. For photoconductive detection, a photoconductive antenna with a photoconductive gap is again used. The probe beam is focused onto the photoconductive gap, which leads to the generation of electron-hole pairs. The simultaneous presence of the electric field from a THz pulse accelerates these electron-hole pairs, and the resulting photocurrent from the antenna is measured, typically by way of phase-sensitive lock-in detection. In this way, the THz electric field is sampled by the probe pulses as a function of the pump-probe time delay (Baxter and Guglietta, 2011). For electro-optic detection, a nonlinear anisotropic crystal is used. Within this electro-optic crystal, the presence of the THz electric field rotates the polarization of a co-propagating probe laser beam. The THz-induced change to the probe laser beam's polarization is then measured as the difference in two (orthogonally-polarized) probe beam powers on balanced photodiodes. The difference in the generated photocurrents is then

recorded as a function of the pump-probe time delay to produce the time-resolved THz waveforms (Gallot and Grischkowsky, 1999).

Overall, it can be said that the above approaches for THz generation and detection have differing performance levels for bandwidth and signal-to-noise ratio (SNR). For the generation, optical rectification often exhibits a wider bandwidth and lower SNR in comparison to photoconductive generation. For the detection, the two approaches often show comparable bandwidth (Kono et al., 2004), although the bandwidth can be improved for electro-optic detection by using a thinner electro-optic crystal (Khiabani et al., 2011; Park et al., 1999). Nonetheless, suchan improvement should only be sought with careful consideration to the SNR, because thinner electro-optic crystals also yield lower signal levels and thus lower SNR values. The general differences in performance for the approaches of THz generation and detection are summarized inTable A.1 by way of radiated power, SNR, and bandwidth.

Table A.1

Performance levels for approaches of THz generation and detection in terms of radiated power, SNR, and bandwidth.

Approaches for THz generation and detection	**Radiated power**	**SNR**	**Bandwidth**
Photoconductive generation	Higher	High	Low
Electro-optic generation	Lower	Low	High
Photoconductive detection	NA	High	Low
Electro-optic detection	NA	Low	High

References

Ajito, K., A., Ueno, Y., 2011. IEEE Trans. Terahertz Sci. Technol. 1, 293–300.

Al-hujazy, R., Collier, C.M., 2018. Photonics. 5, 5, 1–10.

Alfihed, S., Bergen, M.H., Ciocoiu, A., Holzman, J.F., Foulds, I.G., 2018a. Micromachines. 9, 453, 1–9.

Alfihed, S., Bergen, M.H., Holzman, J.F., Foulds, I.G., 2018b. Polymer. 153, 325–330.

Ashworth, P.C., Pickwell-macpherson, E., Provenzano, E., Pinder, S.E., Purushotham, A.D., Pepper, M., Wallace, V.P., 2009. Opt. Express. 17, 93–94.

Baragwanath, A.J., Swift, G.P., Dai, D., Gallant, A.J., Chamberlain, J.M., 2010. J. Appl. Phys. 108, 013102.

Barkal, L.J., Theberge, A.B., Guo, C., Spraker, J., Rappert, L., Berthier, J., Brakke, K.A., Wang, C.C.C., Beebe, D.J., Keller, N.P., Berthier, E., 2016. Nat. Commun. 7, 1–11.

Baxter, J.B., Guglietta, G.W., 2011. Anal. Chem. 83, 4342–4368.

Beard, M.C., Turner, G.M., Schmuttenmaer, C.A., 2002. J. Phys. Chem. B 106, 7146–7159.

Berrier, A., Schaafsma, M.C., Nonglaton, G., Bergquist, J., Rivas, J.G., 2012. Biomed. Opt. Express 3, 2937–2949.

Berry, C.W., Wang, N., Hashemi, M.R., Unlu, M., Jarrahi, M., 2013. Nat. Commun. 4, 1622.

Bershtein, V.A., Ryzhov, V.A., 1994. Far infrared spectroscopy of polymers, in Polymer Analysis and Characterization. Advances in Polymer Science. Springer, Berlin, pp. 43–121.

Berthier, E., Dostie, A.M., Lee, U.N., Berthier, J., Theberge, A.B., 2019. Anal. Bioanal. Chem. 91, 8739–8750.

Berthier, E., Warrick, J., Yu, H., Beebe, D.J., 2008. Lab Chip 8, 852–859.

Bo, S.U., Yaxiong, W.U., Yiwei, W., Jingsuo, H., Shengbo, Z., Cunlin, Z., 2018. Microfluidic chip with sandwich structure for terahertz spectra of glycerol, in: 43rd International Conference on Infrared, Millimeter, and Terahertz Waves (IRMMW-THz).

Burford, N.M., El-shenawee, M.O., 2017. Opt. Eng. 56, 010901.

Cai, Y., Brener, I., Lopata, J., Wynn, J., Pfeiffer, L., Federici, J., 1997. Appl. Phys. Lett. 71, 2076–2078.

Chen, J., Knab, J.R., Cerne, J., Markelz, A.G., 2005. Phys. Rev. E 72.

Cheon, H., Yang, H., Lee, S., Kim, Y.A., Son, J., 2016. Sci. Rep. 6.

Cunningham, P.D., Valdes, N.N., Vallejo, F.A., Hayden, L.M., Polishak, B., Zhou, X.H., Luo, J., Jen, A.K.Y., Williams, J.C., Twieg, R.J., 2011. J. Appl. Phys. 109, 043505.

Dai, J., Zhang, J., Zhang, W., Grischkowsky, D., 2004. J. Opt. Soc. Am. B. 21, 1379–1386.

Dalton,C., Kaler, K.V.I.S., 2007. Sensors Actuators B. Chem. 123, 628–635.

Defonzo, A.P., Lutz, C.R., 1987. Sci. Process. 51, 212–214.

Dhillon, S.S., Vitiello, M.S., Linfield, E.H., Davies, A.G., Hoffmann, M.C., Booske, J., Paoloni, C., Gensch, M., Weightman, P., Williams, G.P., Castro-Camus, E., Cumming, D.R.S., Simoens, F., Escorcia-Carranza, I., Grant, J., Lucyszyn, S., Kuwata-Gonokami, M., Konishi, K., Koch, M.,

Schmuttenmaer, C.A., Cocker, T.L., Huber, R., Markelz, A.G., Taylor, Z.D., Wallace, V.P., Axel Zeitler, J., Sibik, J., Korter, T.M., Ellison, B., Rea, S., Goldsmith, P., Cooper, K.B., Appleby, R., Pardo, D., Huggard, P.G., Krozer, V., Shams, H., Fice, M., Renaud, C., Seeds, A., Stöhr, A., Naftaly, M., Ridler, N., Clarke, R., Cunningham, J.E., Johnston, M.B., 2017. J. Phys. D. Appl. Phys. 50, 043001.

Duvillaret, L., Garet, F. ric, Coutaz, J.-L., 1999. Appl. Opt. 38, 409–415.

Esteves, A.C.C., Brokken-Zijp, J., Laven, J., Huinink, H.P., Reuvers, N.J.W., Van, M.P., de With, G., 2009. Polymer. 50, 3955–3966.

Exter, M. Van, Fattinger, C., Grischkowsky, D., 1989. Opt. Lett. 14, 1128–1130.

Exter, M. van, Grischkowsky, D.R., 1990. IEEE Trans. Microw. Theory Tech. 38, 1684–1691.

Fan, F., Gu, W.H., Wang, X.H., Chang, S.J., 2013. Appl. Phys. Lett. 102.

Fan, N., Su, B., Zhang, C., Zhang, C., 2016. Design and research for biosensing THz microfluidic chips, in: SPIE/COS Photonics Asia.

Ferguson, B., Zhang, X.C., 2002. Nat. Mater. 1, 26–33.

Fischer, B.M., Walther, M., Jepsen, P.U., 2002. Phys. Med. Biol. 47, 3807–3814.

Gallot, G., Grischkowsky, D., 1999. J. Opt. Soc. Am. B. 16, 1204–1212.

George, P.A., Hui, W., Rana, F., Hawkins, B.G., Smith, A.E., Kirby, B.J., 2008. Opt. Express. 16, 1577.

Globus, T., Woolard, D., Crowe, T.W., Gelmont, B., Hesler, J., 2006. J. Phys. D: Appl. Phys. 39, 15.

Globus, T.R., Woolard, D.L., Khromova, T., Crowe, T.W., Gelmont, B.L., Hesler, J., Samuels, A.C., 2003. J. Biol. Phys. 29, 89–100.

Goldstein, Y., Grover, N.B., Chang, C., Jelli, A., Andre, J., Mark, P., Goodwin, A., Mark, P., 1979. IEEE Trans. Electron Devices. 26, 1880–1886.

Grundt, J.A., Ibey, B.L., Liang, M., Wilmink, G.J., 2013. J. of Biomedical Optics. 18, 120503.

Halldorsson, S., Lucumi, E., Gómez-Sjöberg, R., Fleming, R.M.T., 2015. Biosens. Bioelectron. 63, 218–231.

Hu, B.B., Nuss, M.C., 1995. Opt. Lett. 20, 1716–1718.

Jepsen, P.U., Fischer, B.M., 2005. Opt. Lett. 30, 29–31.

Jin, Y., Ma, X.F., Zhang, X., Bliss, D., Larkin, J., Alexander, M., 1994. Appl. Phys. Lett. 64, 1324–1326.

Johnston, I.D., McCluskey, D.K., Tan, C.K.L., Tracey, M.C., 2014. J. Micromechanics Microengineering. 24, 035017.

Khiabani, N., Huang, Y., Shen, Y., 2011. Comparison of Ultra-Wideband THz Generation and Detection Systems, in: Proceedings of the 5th European Conference on Antennas and Propagation (EUCAP). IEEE, pp. 457–461.

Kiwa, T., Oka, S., Kondo, J., Iwao, K., Yamada, H., Tonouchi, M., Tsukada, K., 2007. Jpn. J. Appl. Phys. 46, L1052–L1054.

Kono, S., Tani, M., Sakai, K., 2004. Appl. Phys. Lett. 79, 898.
Lin, Y., Yang, C., Wu, C., Grumezescu, A.M., Wang, C., Hsieh, W., Chen, S., Huang, K., 2013. Molecules 18, 6521–6531.
Lesack, N. I., Fredeen, N. V., Jirasek, A., Holzman, J.F., 2020. IEEE Trans. Terahertz Sci. Technol. 10, 282–291.
Liu, H., Plopper, G., Earley, S., Chen, Y., Ferguson, B., Zhang, X., 2007. Biosens. Bioelectron. 22, 1075–1080.
Liu, L., Jiang, Z., Rahman, S., Shams, M.I. Bin, Jing, B., Kannegulla, A., Cheng, L.J., 2016. Micromachines. 7, 1–10.
Liu, L., Pathak, R., Cheng, L.J., Wang, T., 2013. Sensors Actuators, B Chem. 184, 228–234.
Liu, M., Zhou, D., Zhang, M., Cui, H.L., Wang, D., 2016. A microfluidic chip for terahertz spectral detection, in: IEEE 3M-NANO 2016 - 6th IEEE International Conference on Manipulation, Manufacturing and Measurement on the Nanoscale. pp. 59–63.
Lorenzo Amato, Gu, Y., Bellini, N., Eaton, S.M., Cerulloa, G., Osellame, R., 2012. Lab Chip 12, 1135–1142.
Mark, D., Haeberle, S., Roth, G., Stetten, F. von, Zengerle, R., 2010. Chem. Soc. Rev. 39, 1153–1182.
Markelz, A.G., Roitberg, A., Heilweil, E.J., 2000. Chem. Phys. Lett. 320, 42–48.
McDonald, J.C., Duffy, D.C., Anderson, J.R., Chiu, D.T., Wu, H., Schueller, O.J.A., Whitesides, G.M., 2000. Electrophoresis. 21, 27–40.
Mickan, S., Jingzhou, X., Jesper, M., Zhang, X.-C., Abbott, D., 2003. The limit of spectral resolution in THztime-domain spectroscopy, in: Proceeding of SPIE 5277.
Naftaly, M., Dudley, R., 2009. Opt. Lett. 34, 1213–1215.
Naftaly, M., Miles, R.E., 2007a. Proc. IEEE. 95, 1658–1665.
Naftaly, M., Miles, R.E., 2007b. J. Appl. Phys. 102, 043517.
Naftaly, M., Miles, R.E., 2005. J. Non. Cryst. Solids. 351, 3341–3346.
Nagel, M., Bolivar, P.H., Brucherseifer, M., Kurz, H., 2002. Appl. Phys. Lett. 80, 154–156.
Nazarov, M.M., Shkurinov, A.P., Kuleshov, E.A., Tuchin, V. V, 2008. Quantum Electron. 38, 647–654.
Park, S., Melloch, M.R., Weiner, A.M., 1999. IEEE J. Quantum Electron. 35, 810–819.
Passarelli, M.K., Wang, J., Kurczy, M.E., Ewing, A.G., 2013. Anal. Chem. 85, 522–542.
Philip, E., Parrott, J., Sun, Y., Pickwell-macpherson, E., 2011. J. Mol. Struct. 1006, 66–76.
Png, G.M., Flook, R., Ng, B.W., Abbott, D., 2009. Electronics Letters. 45, 80–81.
Podzorov, A., Gallot, G., 2010. Chem. Phys. Lett. 495, 46–49.
Quan, X., 1989. Polym. Eng. Sci. 29, 1419-1425.
Reid, C.B., Reese, G., Gibson, A.P., Wallace, V.P., 2013. IEEE J. Biomed. Heal. Informatics. 17, 774–778.
Shiraga, K., Ogawa, Y., Suzuki, T., Kondo, N., Irisawa, A., Imamura, M., 2014. J. Infrared,

Millimeter, Terahertz Waves Vol. 35, 493–502.
Scherer, J.R., Paegel, B.M., Wedemayer, G.J., Emrich, C.A., Lo, J., Medintz, I.L., Mathies, R.A., 2001. Biotechniques 31, 1150–1154.
Shumyatsky, P., Alfano, R.R., 2011. J. Biomed. Opt. 16, 033001.
Sirtori, C., 2002. Nature. 417, 132–133.
Smith, P.R., Auston, D.H., 1988. IEEE J. Quantum Electron. 24, 255–260.
Song, Y., Zhao, K., Zuo, J., Wang, C., Li, Y., Miao, X., Zhao, X., 2017. Sensors 17, 2330, 1–10.
Su, B., Zhang, C., Fan, N., Zhang, C., 2016. Terahertz microfluidic chips for detection of amino acids in aqueous solutions, in: SPIE/COS Photonics Asia.
Tang, M., Zhang, M., Yan, S., Xia, L., Yang, Z., Du, C., Cui, H., Wei, D., 2018. PLoS One. 1–12.
Tang, Q., Liang, M., Lu, Y., Wong, P.K., Gerald, J., Tang, Q., Liang, M., Lu, Y., Wong, P.K., Wilmink, G.J., Xin, H., 2013. Development of terahertz (THz) microfluidic devices for "Lab-on-a-Chip" applications, in: SPIE BiOS.
Tang, Q., Liang, M., Lu, Y., Wong, P.K., Wilmink, G.J., Zhang, D., Xin, H., 2016. Sensors. 16, 476, 1–11.
Tani, M., Matsuura, S., Sakai, K., Nakashima, S., 1997. Appl. Opt. 36, 7853–7859.
Tani, M., Yamamoto, K., Estacio, E.S., Que, C.T., Nakajima, H., Hibi, M., Miyamaru, F., Nishizawa, S., Hangyo, M., 2012. J. Infrared, Millimeter, Terahertz Waves. 33, 393–404.
Tsao, C., 2016. Micromachines. 7, 225, 1–11.
Upadhya, P.C., Shen, Y.C., Davies, A.G., Linfield, E.H., 2003. J Biol Phys. 29, 117–121.
Wang, L., Zhou, G., Guan, X., Zhao, L., 2020. Biomol. Spectrosc. 235.
Whitesides, G.M., 2006. Nature. 442, 368–373.
Wietzke, S., Jansen, C., Reuter, M., Jung, T., Kraft, D., Chatterjee, S., Fischer, B.M., Koch, M., 2011. J. Mol. Struct. 1006, 41–51.
Withayachumnankul, W., Fischer, B.M., Abbott, D., 2008a. Opt. Express. 16, 7382.
Withayachumnankul, W., Fischer, B.M., Lin, H., Abbott, D., 2008b. J. Opt. Soc. Am. B 25, 1059–1072.
Withayachumnankul, W., Naftaly, M., 2014. J. Infrared, Millimeter, Terahertz Waves. 35, 610–637.
Withayachumnankul, W., Png, G.M., Yin, X., Atakaramians, S., Jones, I., Lin, H., Seam, B., Ung, Y., Balakrishnan, J., Ng, B.W., Ferguson, B., Mickan, S.P., Fischer, B.M., Abbott, D., 2007. Proc. IEEE 95, 1528–1558.
Yang, K., Yang, X., Zhao, X., Lamy, M., Chapelle, D., Fu, W., 2019. Anal. Chem. 91, 785–791.
Yang, X., Wei, D., Yan, S., Liu, Y., Yu, S., Zhang, M., Yang, Z., Zhu, X., Huang, Q., Cui, H., Fu, W., 2016a. J. Biophotonics 9, 1050–1058.
Yang, X., Yang, K., Zhao, X., Lin, Z., Liu, Z., Luo, S., Zhang, Y., Wang, Y., Fu, W., 2017. Analyst. 142, 4661–4669.

Yang, X., Zhao, X., Yang, K., Liu, Y., Liu, Y., Fu, W., Luo, Y., 2016b. Trends Biotechnol. 34, 810–824.
Yoon, S.A., Cha, S.H., Jun, S.W., Park, S.J., Park, J.-Y., Lee, S., Kim, H.S., Ahn, Y.H., 2020. Biomed. Opt. Express 11, 406–416.
Yu, L., Hao, L., Meiqiong, T., Jiaoqi, H., Wei, L., Jinying, D., Xueping, C., Weiling, F., Yang, Z., 2019. RSC Adv. 9, 9354–9363.
Zhuang, W, Feng, Y, Prohofsky, W.P., 1990. Phys Rev A. 41, 7033.
Yu, Z.T.F., Guan, H., Cheung, M.K., Mchugh, W.M., Cornell, T.T., Shanley, T.P., Kurabayashi, K., Fu, J., 2015. Sci. Rep. 5.
Zhang, C., Durbin, S.M., 2006. J. Phys. Chem. B 110, 23607–23613.